

Thickness dependent exchange bias in martensitic epitaxial Ni-Mn-Sn thin films

Anna Behler, Niclas Teichert, Biswanath Dutta, Anja Waske, Tilmann Hickel, Alexander Auge, Andreas Hütten, and Jürgen Eckert

Citation: *AIP Advances* **3**, 122112 (2013); doi: 10.1063/1.4849795

View online: <https://doi.org/10.1063/1.4849795>

View Table of Contents: <http://aip.scitation.org/toc/adv/3/12>

Published by the [American Institute of Physics](#)

Articles you may be interested in

[Investigations on Ni-Co-Mn-Sn thin films: Effect of substrate temperature and Ar gas pressure on the martensitic transformations and exchange bias properties](#)

AIP Advances **5**, 037108 (2015); 10.1063/1.4914404

[Inverse magnetocaloric effect of epitaxial Ni-Mn-Sn thin films](#)

Applied Physics Letters **103**, 222403 (2013); 10.1063/1.4834357

[Exchange bias effect in martensitic epitaxial Ni-Mn-Sn thin films applied to pin CoFeB/MgO/CoFeB magnetic tunnel junctions](#)

Applied Physics Letters **106**, 192401 (2015); 10.1063/1.4921080

[Exchange bias effect in the martensitic state of Ni-Co-Mn-Sn film](#)

Applied Physics Letters **102**, 232406 (2013); 10.1063/1.4811164

[Epitaxial Ni-Mn-Ga-Co thin films on PMN-PT substrates for multicaloric applications](#)

Journal of Applied Physics **118**, 053906 (2015); 10.1063/1.4927850

[Large reversible magnetocaloric effect in Ni-Mn-In-Co](#)

Applied Physics Letters **106**, 021901 (2015); 10.1063/1.4905371

PHYSICS TODAY

WHITEPAPERS

MANAGER'S GUIDE

Accelerate R&D with
Multiphysics Simulation

READ NOW

PRESENTED BY

 COMSOL

Thickness dependent exchange bias in martensitic epitaxial Ni-Mn-Sn thin films

Anna Behler,^{1,2} Niclas Teichert,³ Biswanath Dutta,⁴ Anja Waske,¹
Tilman Hickel,⁴ Alexander Auge,³ Andreas Hütten,³ and Jürgen Eckert^{1,5}

¹*IFW Dresden, Institute for Complex Materials, P.O. Box 27 01 16, 01171 Dresden, Germany*

²*Department of Physics, Institute for Solid State Physics, Dresden University of Technology, 01062 Dresden, Germany*

³*Department of Physics, Thin Films and Physics of Nanostructures, Bielefeld University, 33501 Bielefeld, Germany*

⁴*Max-Planck Institut für Eisenforschung, 40237 Düsseldorf, Germany*

⁵*Institute of Materials Science, Dresden University of Technology, 01062 Dresden, Germany*

(Received 5 September 2013; accepted 2 December 2013; published online 10 December 2013)

A thickness dependent exchange bias in the low temperature martensitic state of epitaxial Ni-Mn-Sn thin films is found. The effect can be retained down to very small thicknesses. For a Ni₅₀Mn₃₂Sn₁₈ thin film, which does not undergo a martensitic transformation, no exchange bias is observed. Our results suggest that a significant interplay between ferromagnetic and antiferromagnetic regions, which is the origin for exchange bias, is only present in the martensite. The finding is supported by ab initio calculations showing that the antiferromagnetic order is stabilized in the phase. © 2013 Author(s). All article content, except where otherwise noted, is licensed under a Creative Commons Attribution 3.0 Unported License. [<http://dx.doi.org/10.1063/1.4849795>]

In 1956 Meiklejohn and Bean discovered exchange bias (EB) by studying Co particles embedded in their native antiferromagnetic oxide (CoO).¹ Since then the EB itself and the materials exhibiting this effect have been studied extensively in order to evaluate potential applications in spin-electronic devices.² The effect is characterized by a shift of the magnetic hysteresis loops for coupled antiferromagnet-ferromagnet systems when it is cooled through the Néel temperature (T_N) of the antiferromagnet in presence of a magnetic field.^{1,2} The origin of the shift is the unidirectional anisotropy generated by the coupling of ferromagnetic and antiferromagnetic subsystems at their interface. Therefore, the EB is observed in many systems with antiferromagnet-ferromagnet interfaces, such as spin glasses,³ nanoparticles⁴ and bilayers.⁵ Given the trend of miniaturization in electronics, there is currently a focus on the EB effect in small-scale systems such as thin films.

Ferromagnetic shape memory alloys (FSMAs) form another interesting material class with high potential for applications.⁶ One fascinating group of FSMAs are the Ni-Mn-X (X = Sn, In, Ga and Sb) full Heusler alloys, that exhibit multifunctional properties such as magnetic-field induced strain and a large magnetocaloric effect (MCE), both of which are associated with a first-order austenite to martensite structural transition.^{7,8} Detailed studies on the magnetic and structural properties of bulk- and thin-film FSMAs have been reported in literature.^{9,10} In particular, thin-films FSMAs are actively studied for use as microactuators or as high-capacity cooling devices.¹¹

In this paper we have studied in detail the EB effect in the FSMA system Ni-Mn-Sn. For bulk and thick film Ni-Mn-Sn the appearance of EB in the martensitic phase of the system has been reported earlier^{12,13} with varying magnitudes for the hysteresis loop shift. Because such a single-phase system possesses a significant EB it can potentially simplify the production process of EB devices as compared to the conventional process involving a two-layer system. However, the thickness of thin-films plays an important role for many effects and the magnetic properties.¹¹ In previous literature, the influence of the film thickness on EB in thin Ni-Mn-X (X = Sn, In and Sb)

TABLE I. Lattice parameters a of five different Ni-Mn-Sn samples.

	Composition	Thickness d [nm]	Lattice parameter a [nm]
Sample A	Ni ₅₂ Mn _{33.3} Sn _{14.7}	30	0.598
Sample B	Ni _{51.6} Mn _{32.9} Sn _{15.5}	50	0.599
Sample C	Ni _{51.6} Mn _{32.9} Sn _{15.5}	100	0.599
Sample D	Ni _{51.6} Mn _{32.9} Sn _{15.5}	200	0.599
Sample E	Ni ₅₀ Mn ₃₂ Sn ₁₈	100	0.600

systems has not yet been reported. Therefore, we have investigated the EB effect and its dependence on the film thickness in the martensitic state of epitaxial Ni-Mn-Sn thin films. For this purpose, we prepared five Ni-Mn-Sn films varying in composition and in film thickness (cf. Table I).

The thin films were deposited by DC co-sputtering from elemental targets on MgO(001) substrates. The base pressure in the vacuum chamber was typically better than $p_{\text{vac}} = 5 \cdot 10^{-9}$ mbar and the argon pressure during the sputter process was $p_{\text{sputt}} = 2 \cdot 10^{-3}$ mbar. The 3 in. sputter sources were arranged in confocal sputter-up geometry. The inclination angle of the sources was $\alpha = 30^\circ$ and the target to substrate distance was $d_{\text{target}} = 21$ cm. The Ni, Mn and Sn targets had a purity of 4N. The deposition rate was $r = 0.23$ nm \cdot s⁻¹ and during the Ni-Mn-Sn deposition, the temperature of the substrate was $T = 600^\circ\text{C}$. We refer to samples A, B, C and D that were capped by an MgO layer with a thickness of $d_{\text{MgO}} = 2$ nm deposited by e-beam evaporation. The composition and thickness of the films was determined by X-ray fluorescence (XRF) and X-ray reflectivity (XRR) measurements, respectively. The crystal structure was identified by a Philips X'Pert Pro MPD diffractometer using Cu- K_α radiation with $\lambda = 0.15419$ nm at room temperature. The magnetic data were measured using a VSM (PPMS, Quantum Design) in a temperature range $10 \text{ K} \leq T \leq 370 \text{ K}$ and under in-plane magnetic fields from $\mu_0 H = 10$ mT to $\mu_0 H = 1$ T. To determine the coercivity of the magnetic hysteresis, the samples were re-measured using a SQUID magnetometer (MPMS, Quantum Design) to avoid small artifact loop shifts originating from the VSM measurement technique.

The magnetization measurements for zero field cooling (ZFC) and field cooling (FC) were taken in a magnetic field of $\mu_0 H = 10$ mT. For the ZFC curves, the samples were first cooled in zero field from $T = 350$ K to $T = 10$ K and then heated up to 350 K in a field of $\mu_0 H = 10$ mT while recording the data. The FC curves were measured while heating from $T = 10$ K up to $T = 350$ K in a field of $\mu_0 H = 10$ mT after first cooling the samples in a magnetic field with $1 \text{ T} \leq \mu_0 H \leq 5 \text{ T}$ from $T = 350$ K to $T = 10$ K.

The lattice parameters of Ni_{50.000}Mn_{34.375}Sn_{15.625} were calculated using density functional theory with the projector augmented-wave (PAW) method¹⁴ as implemented in the Vienna ab initio simulation package (VASP).¹⁵ We used the generalized gradient approximation (GGA)¹⁶ to calculate the total energies and forces. An energy cutoff of 400 eV is used to truncate the plane wave expansion and a k-point grid of $10 \times 10 \times 10$ is used for Brillouin zone sampling. The Methfessel-Paxton scheme¹⁷ with a width of 0.15 eV is used for the force calculations.

To model the random alloy, we have used the concept of special quasirandom structures (SQS) as proposed by Zunger *et al.*¹⁸ These are specially designed periodic structures that closely mimic the correlation functions of the infinite random substitutional alloys with a limited number of atoms per unit cell. More specifically we have used the Alloy Theoretic Automated Toolkit (ATAT) package¹⁹ to generate a 32-atom SQS of ternary Ni₅₀Mn_{34.375}Sn_{15.625} in which the extra Mn replacing the Sn and mix randomly with the remaining Sn in one sublattice (here, Z sites for $L2_1 X_2 YZ$).

The θ - 2θ scans for both samples (Fig. 1) confirm that an austenitic Ni-Mn-Sn phase is the dominating phase at room temperature.

The indexed austenitic state has a cubic $L2_1$ -type crystal structure with different lattice parameters as shown in Table I.

These results are in good agreement with our DFT calculations on Ni_{50.000}Mn_{34.375}Sn_{15.625}, where at $T = 0$ K we calculated $a = 0.5972$ nm for the lattice constant of the cubic austenite. It was observed in experiments that the lattice parameter for the austenite hardly changes within the

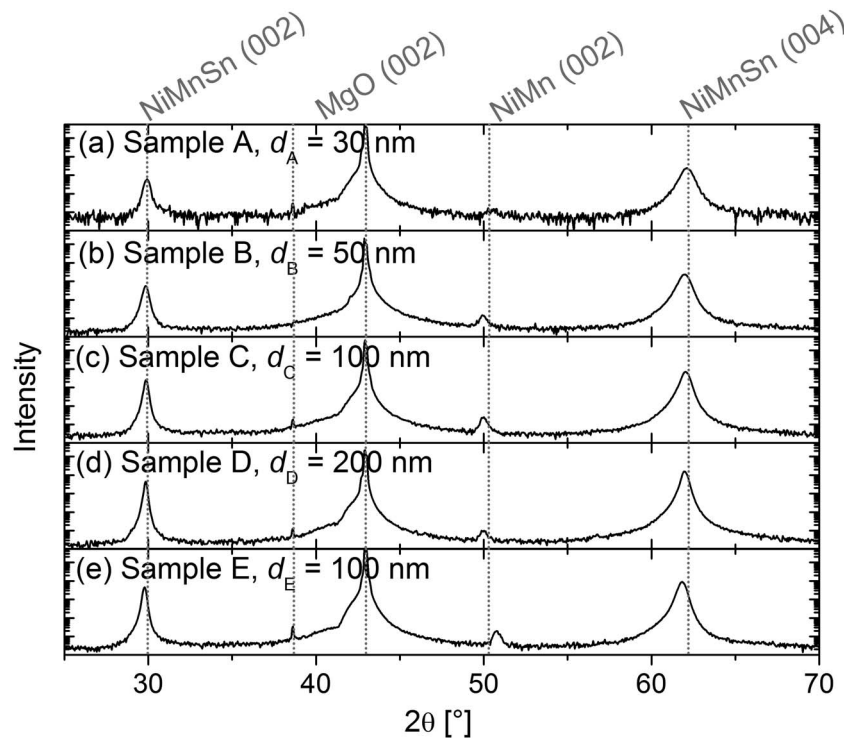


FIG. 1. XRD pattern of a $d_A = 30$ nm (sample A) thick $\text{Ni}_{52}\text{Mn}_{33.3}\text{Sn}_{14.7}$ film, $\text{Ni}_{51.6}\text{Mn}_{32.9}\text{Sn}_{15.5}$ films with thicknesses $d_B = 50$ nm (sample B), $d_C = 100$ nm (sample C), $d_D = 200$ nm (sample D) and a $d_C = 100$ nm thick $\text{Ni}_{50}\text{Mn}_{32}\text{Sn}_{18}$ film (sample E).

temperature interval from $T = 240$ K to $T = 290$ K.²⁰ This provides a basis for the comparability of our calculated lattice constant with the finite temperature experimental results. In all samples a small amount of another phase (XRD peak at $2\theta = 51^\circ$) was present. The data are consistent with an antiferromagnetic $L1_0$ NiMn phase.²¹ Due to 360° ϕ -scans of the (002) peak (not shown), the films can be assumed to be epitaxial.

Figure 2 shows the temperature dependence of the magnetization of all five samples for cooling and heating in a magnetic field of $\mu_0 H = 10$ mT.

The cooling curve of sample A shows a sharp increase of the magnetization with decreasing temperature due to the magnetic transition of the austenitic state with $T_{C,A} = 302$ K (Fig. 2(a)). The magnetization reaches a maximum and decreases upon further cooling until a local minimum is reached. At even lower temperatures the magnetization increases again. The origin of this behavior is a structural transition from the austenite to the martensite state, which is superposed with a magnetic transition in the martensite state. Below $T = 110$ K the magnetization is constant. Furthermore, the heating and the cooling curves show a hysteresis between $T = 135$ K and $T = 273$ K, which can be ascribed to a first-order structural transition. The maximum close to $T_{C,A}$ of the heating curve does not reach the value obtained during cooling due to the fact that the magnetic transition of the austenitic state (i.e. a decrease of magnetization at $T_{C,A}$) superposes the structural transition from martensite to austenite. Samples B, C and D show a similar temperature dependent behavior of the magnetization as sample A (Fig. 2(b)–2(d)). Sample B undergoes the paramagnetic to ferromagnetic transition at $T_{C,B} = 308$ K. The magnetization curves again show differences between the heating and cooling curves due to the structural transition from austenite to martensite, which is associated with hysteresis. In the case of samples C and D the structural transition can be better resolved. During cooling, the alloys transform from paramagnetic austenite to ferromagnetic austenite ($T_{C,C} = T_{C,D} = 307$ K), followed by a structural transition into a ferromagnetic martensite. Additionally to the superposition of structural and magnetic transition, the shape of the hysteresis is influenced by the grain size and the number of grain boundaries in the thin films. For similar Ni-Mn-Sn thin

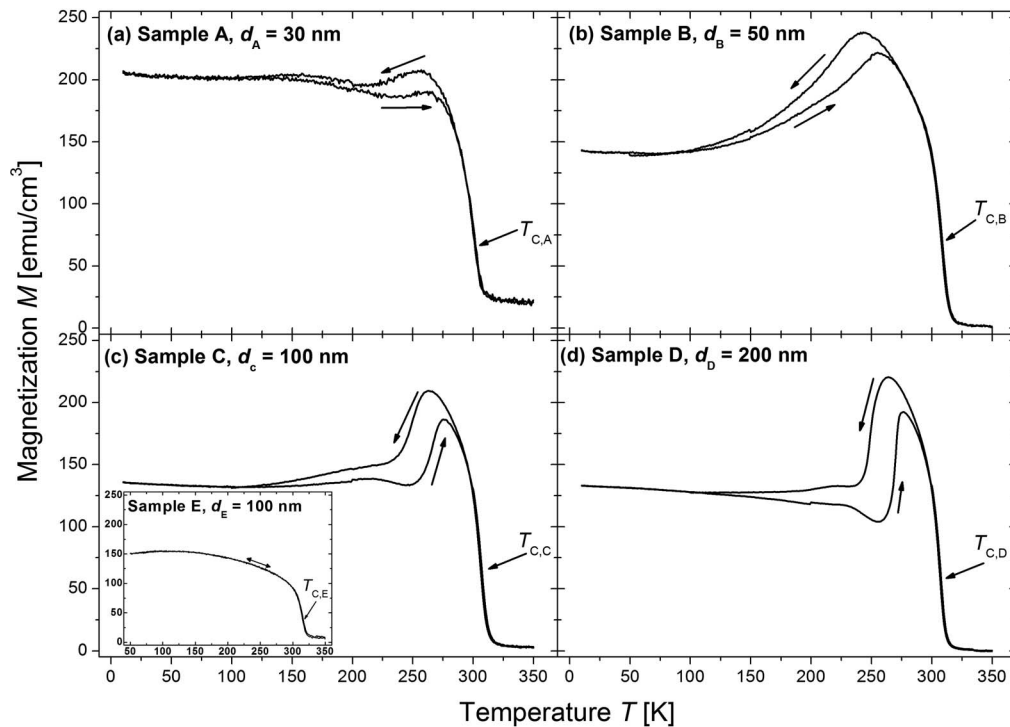


FIG. 2. Temperature dependence (cooling and heating) of the magnetization of a (a) $d_A = 30$ nm (sample A), (b) $d_B = 50$ nm (sample B), (c) $d_C = 100$ nm (sample C) and (d) $d_D = 200$ nm thick (sample D) NiMnSn film under a magnetic field of $\mu_0 H = 10$ mT. The inset of (c) shows the temperature dependent magnetization of sample E ($d_E = 100$ nm).

films was shown that in thin films which showed just a slight signature of the phase transformation (c.f. Fig. 2(a)), the transformation was hindered by a large number of grain boundaries.²² With increasing film thickness the grain size increases and from a certain value for the grain size a complete martensitic transformation can take place. This can be seen in a well-shaped hysteresis (c.f. Fig. 2(d)). The magnetic behavior of sample E (inset of Fig. 2(c)) differs significantly. The curve shows a magnetic transition from paramagnetic to ferromagnetic phase with $T_{C,E} = 316$ K. Due to the fact that there are no deviations between the magnetization while cooling and heating, we conclude that sample E does not undergo a structural transition because of the enhanced Sn content in comparison to the other samples.⁶

For a better understanding of the magnetic interaction in these alloys, we measured ZFC and FC ($\mu_0 H_{FC} = 1$ T) heating curves of the magnetization in a magnetic field of $\mu_0 H = 10$ mT (Fig. 3).

In the region of the martensitic state the ZFC and the FC curves of samples A-D differ significantly (Fig. 3(a)–3(d)). After ZFC of sample A and B the magnetization is nearly constant until $T = 50$ K with increasing temperature (Fig. 3(a)). With further heating the magnetization increases. The slope of the magnetization changes at $T = 200$ K for sample B. Heating above $T = 270$ K in the case of sample A and above $T = 250$ K for sample B induces the magnetic transition from ferromagnetic to paramagnetic phase. In contrast, the magnetization of the FC heating curve decreases with increasing temperature over the same range. In the case of sample A the slope of the magnetization changes above $T = 200$ K. From approximately $T = 300$ K (sample A) and $T = 255$ K onwards both curves lie on top of each other. For samples C and D, the structural transition can be resolved in the magnetic measurements (Fig. 2(c) and 2(d)). It can be seen that a difference between ZFC and FC curves occurs below the temperature at which the martensite to austenite transformation starts and thereby the magnetization increases. After the samples start to transform into the austenitic state the curves in both cases are coincident. Below the martensite start temperature the magnetization after FC decreases while heating. The magnetization after ZFC is constant below $T = 50$ K. With further

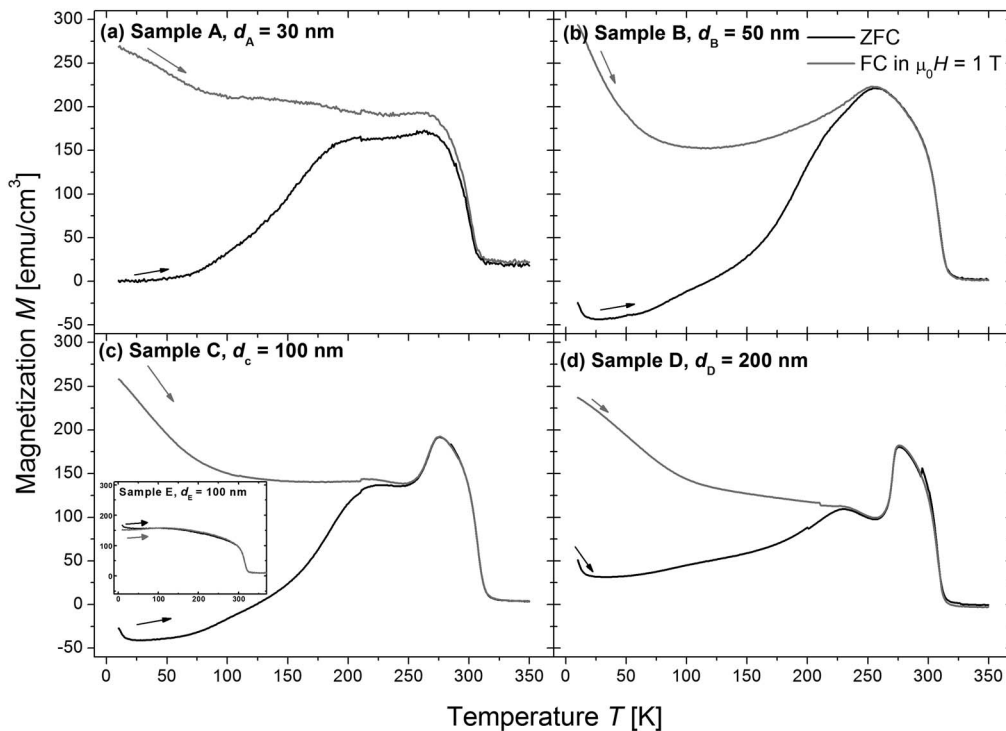


FIG. 3. Temperature dependent magnetization after ZFC and FC of $\text{Ni}_{52}\text{Mn}_{33.3}\text{Sn}_{14.7}$ and $\text{Ni}_{51.6}\text{Mn}_{32.9}\text{Sn}_{15.5}$ films with (a) $d_A = 30$ nm (sample A), (b) $d_B = 50$ nm (sample B), (c) $d_C = 100$ nm (sample C) and (d) $d_D = 200$ nm (sample D) under a magnetic field of $\mu_0 H = 10$ mT. The magnetization (measured under the same conditions) of the $\text{Ni}_{50}\text{Mn}_{32}\text{Sn}_{18}$ ($d_E = 100$ nm) film (sample E) is shown as inset in (c).

heating the magnetization increases. The ZFC heating data of samples B-E below $T = 20$ K are influenced by paramagnetic contamination of the substrate through Fe atoms.

We attribute the origin of difference between the two curves to the existence of different magnetic phases during ZFC and FC. It was observed experimentally by neutron diffraction for Mn-rich Ni-Mn-Sn alloys that the Mn atoms on regular Mn sites have ferromagnetic (FM) interactions between each other and the Mn atoms that are occupying the Sn sites have antiferromagnetic (AFM) interactions to the surrounding Mn atoms.²³ The different interactions between the Mn atoms lead to the assumption that two inhomogeneously distributed magnetic phases (AFM and FM) coexist.¹⁰ The cooling of the system leads to the pinning of the FM regions by neighboring AFM ones. As a consequence after cooling in the absence of an external magnetic field the overall magnetization averages to zero due to the AFM interactions. In the case of field cooling the system, the FM domains become pinned in several directions, inter alia along the external field direction. The increase of the magnetization after ZFC above approximately $T = 50$ K with increasing temperature indicates that this pinning loses dominance. We interpret this temperature as the blocking temperature T_B ; for $T > T_B$ the EB effect vanishes.

To investigate the role of the minority NiMn (cf. x-ray scans Fig. 1), which could in principle also yield AFM contributions, we additionally measured ZFC heating and FC heating curves for sample E (Inset of Fig. 3(c)). Note that there is no structural transition present in this thin film. In distinction to samples A-D, the magnetization curves after ZFC and FC of sample E do not show any difference. Although there is an AFM minority phase embedded in the FM austenite of sample E, there is no appearance of EB in this sample. This leads us to the conclusion that the martensitic transition in samples A-D is needed for EB in this single-layer system and that the NiMn phase can be excluded as a source of the EB effect.

To get a clearer picture on the role of the martensitic transition for the occurrence of EB effect, we have also employed ab initio based computational methods. The motive is to understand

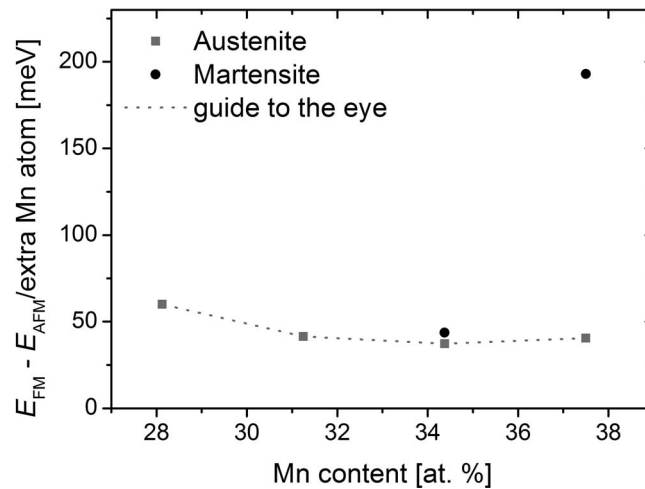


FIG. 4. Energy required to flip the spin of one extra Mn atom sitting on the Sn sub-lattice for the austenite and martensite state in a $Ni_{50}Mn_xSn_{50-x}$ alloy.

the mechanism that suppresses EB in the austenite state. For such a study, we have chosen four different compositions, which are $Ni_{50}Mn_{28.125}Sn_{21.875}$, $Ni_{50}Mn_{31.25}Sn_{18.75}$, $Ni_{50}Mn_{34.375}Sn_{15.625}$ and $Ni_{50}Mn_{37.5}Sn_{12.5}$. In order to simulate the off-stoichiometric compositions, we have constructed an SQS for each composition. As already discussed above, the extra Mn atoms sitting on the Sn sub-lattice are in the ground-state arrangement antiferromagnetically coupled to the Mn atoms sitting on the Mn sub-lattice, which is decisive for the EB. In order to estimate the stability of the AFM configuration in presence of an external magnetic field, we have considered two different orientations of the magnetic moments for the excess Mn atoms occupying the Sn sub-lattice: in the first case, we have considered the ground-state AFM, whereas in the second case, the orientation between the Mn atoms sitting on different sub-lattices is FM.

We have calculated the equilibrium lattice parameters for the cubic austenite state for all four compositions and for the martensite state for those compositions at which the state is formed. In our calculations a clear martensite state is only observed for the $Ni_{50}Mn_{37.5}Sn_{12.5}$ composition, which has a tetragonal structure with $c/a = 1.29$. The $Ni_{50}Mn_{34.375}Sn_{15.625}$ composition is at the edge of the stability region of the martensite state with slight tetragonal deformation ($c/a = 1.01$). For those crystal structures, we have calculated the energy difference between the two different magnetic configurations in both austenite and martensite states. It can be seen in Fig. 4 that the energy required to flip the spin of one extra Mn atom sitting on the Sn sub-lattice never exceeds 60 meV for the austenite state at any composition. On the other hand, similar calculations for the martensite state of $Ni_{50}Mn_{37.5}Sn_{12.5}$ gives an energy difference of 193 meV, which is more than three-fold the value of the austenite state. For $Ni_{50}Mn_{34.375}Sn_{15.625}$ the energy difference to the austenite is not that high due to the small tetragonal deformation in this case. These results suggest that the martensitic transition stabilizes the AFM spin configuration for the extra Mn atoms sitting on Sn sub-lattice. Since the energy required to change the magnetic configuration for the extra Mn atoms on Sn sub-lattice from AFM to FM is rather low in the austenite state, the atoms will more easily follow an external magnetic field. Hence, the exchange bias will be suppressed in this case. In contrast to that, the required energy to change the magnetic configuration is much higher in the martensite state. Therefore, an external magnetic field will mainly influence the FM regions, whereas the AFM regions will remain unaffected. Hence, FM and AFM regions can coexist and couple in the martensite state and thus an EB effect is observed.

To confirm the exchange bias effect we measured magnetization hysteresis loops at $T = 10$ K after ZFC which are shown in Fig. 5.

The magnetic hysteresis loops of samples A, B, C and D are clearly shifted along the positive magnetic field axis. The values of the EB field are calculated using $H_{EB} = |H_{C1} + H_{C2}|/2$, where H_{C1}

TABLE II. Comparison of composition, thickness, EB field and coercivity of different Ni-Mn-Sn thin film samples.

	Composition	d [nm]	$\mu_0 H_{EB, ZFC}$ [mT]	$\mu_0 H_{C, ZFC}$ [mT]
Sample A	Ni ₅₂ Mn _{33.3} Sn _{14.7}	30	14	6.6
Sample B	Ni _{51.6} Mn _{32.9} Sn _{15.5}	50	28.9	9.3
Sample C	Ni _{51.6} Mn _{32.9} Sn _{15.5}	100	34.7	13.1
Sample D	Ni _{51.6} Mn _{32.9} Sn _{15.5}	200	43.4	30.1

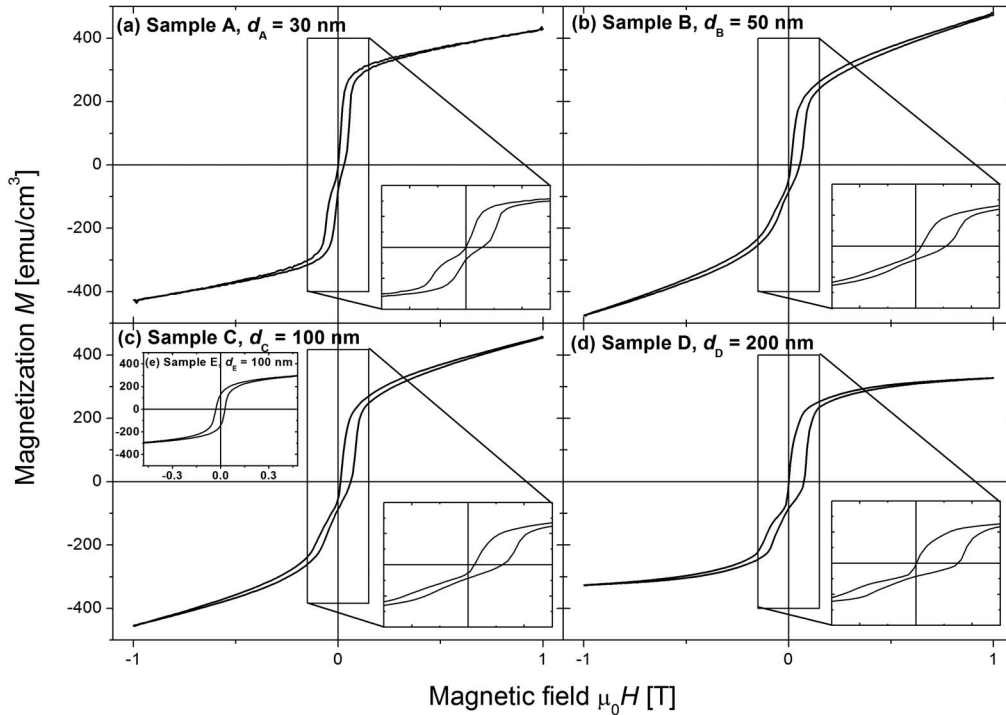


FIG. 5. Magnetization hysteresis loops of (a) a Ni₅₂Mn_{33.3}Sn_{14.7} thin films ($d_A = 30$ nm), (b–d) Ni_{51.6}Mn_{32.9}Sn_{15.5} films ($d_B = 50$ nm, $d_C = 100$ nm and $d_D = 200$ nm) and (e) a Ni₅₀Mn₃₂Sn₁₈ ($d_E = 100$ nm) film measured at 10 K after ZFC (VSM measurements). The insets show an enlarged view of the central region of the loops.

and H_{C2} are the magnetic fields at which the magnetization becomes zero (H_{C1} and H_{C2} are taken from SQUID measurements, not shown). The EB fields for samples A–D are shown in Table II and Fig. 6. H_{EB} shows a dependence on the film thickness. While decreasing the thickness, the value of the loop shift also decreases. However, a strong unidirectional anisotropy can be observed down to very thin films. As expected, the hysteresis loop of sample E is not shifted due to the fact that in this sample EB is not present. The hysteresis loops of samples A, B, C and D differ in their shape from the one of sample E. In the case of samples A–D the magnetization hysteresis after ZFC has a double-shifted shape, which is usually observed in EB systems.²⁴ The double-shifted shape occurs due to an imprint of FM domains into the AFM regions during ZFC. Above T_B , the FM regions align along different directions. During cooling through T_B the imprint of these domains divides the AFM regions also into two types with opposite directions of the axis of the AFM moments. Below T_B each of these regions couples in a different way to the ferromagnet during the hysteresis loop which leads to a double-shifted shaped loop. In comparison, the hysteresis loop after ZFC of sample E is a “normal” shaped one. Since EB does not exist in this sample, the AFM domains will not be imprinted into the FM during cooling.

The values of the coercivity (Table II) are calculated using $H_C = (H_{C2} - H_{C1})/2$. The coercivity of samples A–D also shows clear thickness dependence. With decreasing thickness, the coercivity decreases.

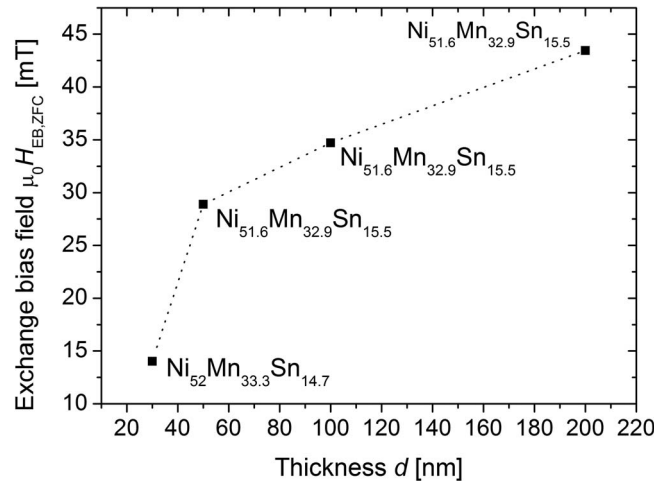


FIG. 6. Thickness dependence of the exchange bias field after ZFC.

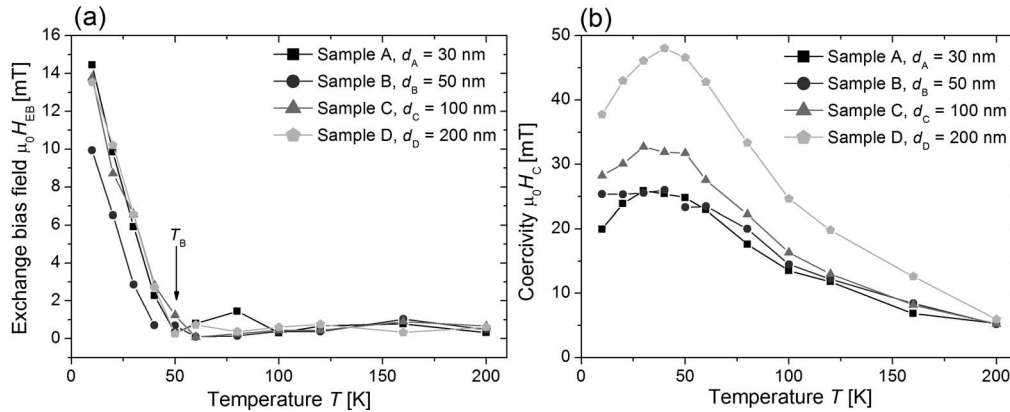
FIG. 7. Temperature dependence after FC in $\mu_0 H = 1$ T of the exchange bias field H_{EB} and coercivity H_C for NiMnSn alloys with different thicknesses.

Figure 7 shows the effect of temperature on the EB field H_{EB} and the coercivity H_C of samples A-D after FC in $\mu_0 H = 1$ T.

The EB field H_{EB} (Fig. 7(a)) of all samples decreases almost linearly with increasing temperature until it disappears at $T_B = 50$ K. The loop shifts at $T = 10$ K after FC are comparable with reported values for $\text{Ni}_{50}\text{Mn}_{36}\text{Sn}_{14}$ bulk ($H_{EB} = 17.5$ mT).¹² Smaller EB fields after FC at $T = 10$ K for films samples, which was reported for a $\text{Ni}_{49.8}\text{Mn}_{36.1}\text{Sn}_{13.9}$ thick film ($d \approx 1 \mu\text{m}$, $H_{EB} = 4.1$ mT),¹³ were not found.

The coercivity H_C (Fig. 7(b)) increases first with increasing temperature and reaches a maximum close to T_B in all cases. This peak is probably a result of the influence of the AFM anisotropy on the coercivity.² Usually in EB systems the AFM anisotropy decreases close to T_B . Thereby rotating FM spins are able to drag AFM spins irreversibly and the coercivity increases. For temperatures above T_B the coercivity decreases, because the AFM orientation is random and does not hinder the FM rotation.²⁵ The thickness dependence of the coercivity is not influenced whether the samples are FC or ZFC. In contrast to this, the thickness dependence gets lost for the EB effect in the FC case.

To investigate the influence of higher H_{FC} values on H_{EB} and H_C , we measured hysteresis loops at $T = 10$ K after FC the samples in $\mu_0 H = 2$ T, 3 T, 4 T and 5 T. We determined that H_{EB} and H_C remain constant, and are independent of H_{FC} .

In conclusion, we observe EB in the martensitic state of a $\text{Ni}_{52}\text{Mn}_{33.3}\text{Sn}_{14.7}$ thin film with $d_A = 30$ nm and in the martensitic state of $\text{Ni}_{51.6}\text{Mn}_{32.9}\text{Sn}_{15.5}$ thin films with $d_B = 50$ nm,

$d_C = 100$ nm and $d_D = 200$ nm (cf. Table II). Due to the very similar chemical compositions we treated them as a thickness dependent film series, independent of their compositions. The EB behavior in the low temperature martensitic state is attributed to the unidirectional anisotropy due to the coupling between FM and AFM interactions. With ab initio based computational methods we explain qualitatively that the martensitic state is favorable for EB as compared to the austenitic state.

We found a thickness dependence of H_{EB} after ZFC. The thickest measured sample shows a loop shift of $H_{EB, ZFC} = 43.4$ mT. This value decreases with decreasing thickness, but it is still of comparable magnitude down to the thinnest sample. For H_{EB} and H_C we found in the samples a strong dependence on temperature. The blocking temperatures are found to be $T_B = 50$ K for all thicknesses. The hysteresis loop of these Ni-Mn-Sn samples in the martensitic state show a double shifted shape at $T = 10$ K after ZFC due to the existence of EB. To exclude the role of the minority NiMn phase, we showed that there was no sign for EB behavior in a $Ni_{50}Mn_{32}Sn_{18}$ ($d_E = 100$ nm) sample without a martensitic transition. These experimental facts, together with ab initio calculations, lead us to the conclusion that a martensitic transition is needed for EB in Ni-Mn-Sn.

ACKNOWLEDGMENTS

The authors thank R. Niemann, S. Fähler and J. D. Moore for helpful discussions. This work is supported by DFG through SPP 1599.

- ¹W. H. Meiklejohn and C. P. Bean, *Phys. Rev.* **102**, 1413 (1956).
- ²J. Nogués and I. K. Schuller, *J. Magn. Magn. Mater.* **192**, 203 (1999).
- ³T. Iwata, K. Kai, T. Nakamichi, and M. Yamamoto, *J. Phys. Soc. Japan* **28**, 582 (1970).
- ⁴J. Nogués, J. Sort, V. Langlais, V. Skumryev, S. Surinach, J. S. Muñoz, and M. D. Baro, *Phys. Rep.* **422**, 65 (2005).
- ⁵R. Jungblut, R. Coehoorn, M. T. Johnson, J. van de Stegge, and A. Reinders, *J. Appl. Phys.* **75**, 6659 (1994).
- ⁶Y. Sutou, Y. Imano, N. Koeda, T. Omori, R. Kainuma, K. Ishida, and K. Oikawa, *Appl. Phys. Lett.* **85**, 4358 (2004).
- ⁷K. Ullakko, J. K. Huang, C. Kantner, R. C. O'Handley, and V. V. Kokorin, *Appl. Phys. Lett.* **69**, 1966 (1996).
- ⁸T. Krenke, E. Duman, M. Acet, E. F. Wassermann, X. Moya, L. Manosa, and A. Planes, *Nature Materials* **4**, 450–454, (2005).
- ⁹R. Niemann, O. Heczko, L. Schultz, and S. Fähler, *Appl. Phys. Lett.* **97**, 222507 (2010).
- ¹⁰T. Krenke, M. Acet, E. F. Wassermann, X. Moya, L. Manosa, and A. Planes, *Phys. Rev. B* **72**, 014412 (2005).
- ¹¹A. Auge, N. Teichert, M. Meinert, G. Reiss, A. Hütten, E. Yuzuak, I. Dincer, Y. Elerman, I. Ennen, and P. Schattschneider, *Phys. Rev. B* **85**, 21 (2012).
- ¹²Z. Li, C. Jing, J. Chen, S. Yuan, S. Cao, and J. Zhang, *Appl. Phys. Lett.* **91**, 112505 (2007).
- ¹³R. Vishnoi and D. Kaur, *J. Alloys Compd.* **509**, 2833 (2011).
- ¹⁴P. E. Bloechl, *Phys. Rev. B* **50**, 17953 (1994).
- ¹⁵G. Kresse and J. Furthmüller, *Phys. Rev. B* **54**, 11169 (1996).
- ¹⁶J. P. Perdew, K. Burke, and M. Ernzerhof, *Phys. Rev. Lett.* **77**, 3865 (1996).
- ¹⁷M. Methfessel and A. T. Paxton, *Phys. Rev. B* **40**, 3616 (1989).
- ¹⁸A. Zunger, S. H. Wei, L. G. Ferreira, and J. E. Bernard, *Phys. Rev. Lett.* **65**, 353 (1990).
- ¹⁹A. van de Walle and G. Ceder, *J. Phase Equilib.* **23**, 348 (2002).
- ²⁰T. Kanomata, K. Fukushima, H. Nishihara, R. Kainuma, W. Itoh, K. Oikawa, K. Ishida, K. U. Neumann, and K. R. A. Ziebeck, *Materials Science Forum* **583**, 119–129 (2008).
- ²¹M. Huang, *J. Appl. Phys.* **97**, 064906 (2005).
- ²²R. Vishnoi, R. Singhal, and D. Kaur, *J. Nanopart. Res.* **13**, 3975 (2011).
- ²³C. V. Stager and C. C. M. Campbell, *Can. J. Phys.* **56**, 674 (1978).
- ²⁴S. Brück, J. Sort, V. Baltz, S. Surinach, J. S. Muñoz, B. Dieny, and M. D. Baro, *J. Nogués, Adv. Mater.* **17**, 2978 (2005).
- ²⁵J. Hu, G. Jin, A. Hu, and Y. Ma, *Eur. Phys. J. B* **40**, 265–271 (2004).